Control Engineering Practice 92 (2019) 104134

Contents lists available at ScienceDirect

Control Engineering Practice

journal homepage: www.elsevier.com/locate/conengprac

Attitude estimation using high-grade gyroscopes

Joel Reis [a,*], Pedro Batista [b], Paulo Oliveira [b,c], Carlos Silvestre [a,1]

[a] Faculty of Science and Technology, University of Macau, Taipa, Macao
[b] Institute for Systems and Robotics, Instituto Superior Técnico, Universidade de Lisboa, Lisboa 1049-001, Portugal
[c] LAETA—Associated Laboratory for Energy, Transports and Aeronautics, IDMEC—Institute of Mechanical Engineering, Instituto Superior Técnico, Universidade de Lisboa, Lisboa 1049-001, Portugal

ARTICLE INFO

Keywords:
Attitude observer
Special orthogonal group
Kalman filter
Inertial reference vector
Earth angular rotation

ABSTRACT

This paper addresses the problem of attitude estimation using the angular velocity of Earth as a reference vector. A nonlinear observer is proposed that evolves on the special orthogonal group and is aided by angular velocity readings containing implicit measurements of the Earth's spin. Additionally, the observer resorts to body-fixed measurements of one constant inertial reference vector. The observer's sole tuning parameter, shaped as a matrix gain, is computed from a time-varying Kalman filter strategically applied to a uniformly observable linear time-invariant system, which is obtained from the linearized rotation matrix error dynamics. The nonlinear observer is proved to be locally exponentially stable but, most noticeably, in spite of this local-based inception, a Monte Carlo simulation analysis demonstrates the good properties of the observer in terms of convergence rate, tuning capability, and large basin of attraction. Furthermore, extensive experimental results confirm the properties of the proposed technique and validate its usage in real world applications.

1. Introduction

The Kalman filter has been the workhorse of a plethora of invaluable contributions to the scientific community, persistently finding its application in virtually all engineering domains (Grewal & Andrews, 2010). The branch of attitude estimation is arguably where the Kalman filter became the most prolific, thanks in part to its quick dissemination and extraordinary achievements in the period known as Space Race. Indeed, during the two decades that followed Wahba's seminal satellite attitude determination problem (Wahba, 1965), several techniques were developed for spacecraft attitude estimation that relied on the celebrated Kalman filter and its variations (Lefferts, Markley, & Shuster, 1982). Soon after this chapter, the advent of affordable unmanned vehicles and the production of commercial low-cost sensors triggered a new wave of attitude estimation techniques based on the Kalman filter that has endured until the present day. Among a wide literature on the subject, see, e.g., the works in Bijker and Steyn (2008), Chang, Hu, and Li (2016), Choukroun, Bar-Itzhack, and Oshman (2006), de Marina, Pereda, Giron-Sierra, and Espinosa (2012), Sabatini (2011) and references therein.

Conceptually, the rotation matrix cannot be uniquely determined with only one reference vector. In order to resolve the orientation ambiguity, a second reference vector is required. In attitude estimation/filtering problems, the objective consists typically in determining the rotation matrix between two frames using inertial information of at least two non-collinear reference vectors and their respective measurements; see, for instance, the works in Batista, Silvestre, and Oliveira (2012), Chang, Qin, and Li (2015), Grip, Fossen, Johansen, and Saberi (2012), Markley (1998), Oshman and Markley (1999) and Wu, Zhou, Gao, Li, Cheng, and Fourati (2018). Accelerometers and magnetometers, despite their inherent limitations (Bachmann, Yun, & Brumfield, 2007), are recurrent sensors used extensively across numerous applications mainly due to their reduced dimensions, performance, and the fact that the gravitational and magnetic fields are known with extreme precision. Gyro-compasses also pose an attractive choice, as they can find the true North direction based on Earth's rotation, and are immune to magnetic field anomalies.

However, it might occur that only one reference vector is available, for instance, in scenarios where vehicles, equipped with both accelerometers and magnetometers, either describe highly accelerated trajectories or happen to be within range of strong magnetic anomalies, therefore preventing the simultaneous use of two reference vectors. In that case, one can use the Kalman filter to overcome the single vector drawback, although it does not guarantee asymptotic stability or even boundedness of errors (Khosravian & Namvar, 2012). Moreover, the structural nature of the Kalman filter forces the lifting of topological constraints, whereby attitude estimations do not evolve on the special

* Corresponding author.
E-mail addresses: joelreis@um.edu.mo (J. Reis), pbatista@isr.tecnico.ulisboa.pt (P. Batista), paulo.j.oliveira@tecnico.ulisboa.pt (P. Oliveira), csilvestre@um.edu.mo (C. Silvestre).
[1] On leave from Instituto Superior Técnico, Universidade de Lisboa, Portugal.

https://doi.org/10.1016/j.conengprac.2019.104134
Received 7 May 2019; Received in revised form 25 July 2019; Accepted 26 August 2019
Available online xxxx
0967-0661/

orthogonal group, also known as the rotational group. In Barrau and Bonnabel (2017), the authors analyze the convergence aspects of the invariant extended Kalman filter when it is used as a deterministic nonlinear observer on Lie groups. More recently, in Stovner, Johansen, Fossen, and Schjølberg (2018), a multiplicative exogenous Kalman filter is presented that employs an attitude representation of minimal degree; offers global exponential stability guarantees; and, contrasts with its extended counterpart by linearizing the nonlinear model about an exogenous signal, therefore replacing the potentially destabilizing feedback with a feedforward from an auxiliary estimator.

The Kalman-based attitude estimation solutions that are available in the literature invariably end up being some modification of the renowned algorithm. To the best of the authors' knowledge, there exist no solutions, developed on the special orthogonal group, that resort solely to the theory of the linear Kalman filter while simultaneously using explicit information about only one reference vector.

In this paper, building upon the work developed in Reis, Batista, Oliveira, and Silvestre (2018) and Reis, Batista, Oliveira, and Silvestre (2019), a novel observer is presented that estimates the rotation matrix based on explicit measurements of one constant inertial reference vector in addition to implicit measurements of the Earth's rotation. Furthermore, the observer's correction term is affected by a gain that can be computed through the application of a linear Kalman filter. The Luenberger like nature of the observer proposed in Reis et al. (2018) and Reis et al. (2019) yields a more straightforward gain tuning, without any reference to a Riccati differential equation. However, the performance of that observer is extremely slow, exhibiting convergence rates of up to a dozen of hours.

The algorithm developed in this paper is nonetheless simple and easy to tune as well, excelling in its performance, which outdoes the performances illustrated in previous works by the authors, in particular (Batista, Silvestre, & Oliveira, 2019a) and Batista, Silvestre, and Oliveira (2019b). In the former, a globally exponentially stable cascade observer explicitly estimates the Earth's angular velocity, and then estimates the rotation matrix without topological constraints. In Batista et al. (2019b), a cascade semi-global attitude observer built on the special orthogonal group was presented that is also based on explicit measurements of a single body-fixed vector. Most noticeably, whereas in both (Batista et al., 2019a) and Batista et al. (2019b) a set of piecewise observer gains had to be tuned in order to ensure both fast convergence speed and good steady-state performance, the Kalman filter in this paper entails a much simpler and straightforward tuning process through its covariance matrices, therefore bypassing the need for piecewise gains. Moreover, much faster convergence is still achieved with the solution proposed herein. However, in this particular work, due to the intricate process of analytically computing a closed-form solution of the Riccati differential matrix equation, only local exponential stability guarantees are provided. Nevertheless, extensive simulation and experimental results are given that demonstrate the effectiveness of the proposed observer with a very large basin of attraction. Still, it urges to emphasize that, in Batista et al. (2019a), the observability analysis of the system was already carried out, with the system shown to be observable.

The rest of the paper is organized as follows: in Section 2 an overview of the problem statement is presented followed by steps leading to the proposed nonlinear attitude estimation solution. Section 3 shows how to compute the observer gain, specifically how the gain can be obtained from the solution of the Riccati differential matrix equation, and addresses the local stability properties of the observer. In Section 4, an extensive performance analysis is carried out through a set of simulations that include Monte Carlo runs. Section 5 includes experimental results that further validate the effectiveness of the proposed observer when tested under real world mission scenarios. Finally, conclusions and some discussions are presented in Section 6.

1.1. Notation

Throughout the paper, a bold symbol stands for a multidimensional variable, the symbol $\mathbf{0}$ denotes a matrix of zeros and $\mathbf{I}$ an identity matrix, both of appropriate dimensions. A positive definite matrix $\mathbf{M}$ is denoted by $\mathbf{M} \succ \mathbf{0}$. $\mathcal{N}(\boldsymbol{\mu}, \boldsymbol{\Sigma})$ stands for a multi-variate normal distribution with mean $\boldsymbol{\mu}$ and covariance $\boldsymbol{\Sigma} \succ \mathbf{0}$. The determinant function of a matrix is represented by $\det(\cdot)$. The Special Orthogonal Group is denoted by $SO(3) := \{\mathbf{X} \in \mathbb{R}^{3\times3} : \mathbf{X}\mathbf{X}^T = \mathbf{X}^T\mathbf{X} = \mathbf{I} \wedge \det(\mathbf{X}) = 1\}$. The skew-symmetric matrix of a vector $\mathbf{a} \in \mathbb{R}^3$ is defined as $\mathbf{S}(\mathbf{a})$, such that given another vector $\mathbf{b} \in \mathbb{R}^3$ one has $\mathbf{a} \times \mathbf{b} = \mathbf{S}(\mathbf{a})\mathbf{b}$. Finally, for convenience, the transpose operator is denoted by the superscript $(\cdot)^T$.

2. Design of attitude observer

2.1. Problem statement

Consider a vehicle or a robotic platform describing a three-dimensional rotational motion in a dynamic environment, and further assume that the vehicle is equipped with a set of three high-grade, orthogonally mounted rate gyros that are accurate enough to be sensitive to the angular velocity of the planet, e.g., the commercial off-the-shelf premium high-performance KVH 1775 inertial measurement unit (IMU) available from KVH Industries, which includes a trio of fiber optic gyros (FOGs) enclosed in a compact design, weighing approximately 700 grams. Moreover, consider two frames, one inertial and another fixed to the vehicle's body. Suppose that the vehicle is equipped with a sensor capable of measuring a reference vector, expressed on the body frame, that is constant when expressed in inertial coordinates. Since the 1775 IMU also features a set of both tri-axial magnetometers and accelerometers, it wholly comprehends the measurements required by the problem.

Therefore, the objective is to determine the rotation matrix from the body frame to the inertial one using angular velocity readings from the high-grade gyros, which implicitly measure the speed of Earth's revolution, in addition to the body-fixed measurements of the reference vector. As opposed to most solutions found in the literature, the observer presented in this paper, which builds upon (Reis et al., 2018) and Reis et al. (2019), resorts to just one measured body-fixed vector while simultaneously preserving topological properties, thus entailing a rather simplified setup design. Moreover, the body-fixed vector that is measured is actually constant in inertial coordinates.

2.2. Observer for the orientation matrix

Let $\mathbf{R}(t) \in SO(3)$ denote the rotation matrix from a body-fixed frame $\{B\}$ to a local North-East-Down (NED) fixed system $\{I\}$.[2] The derivative of this matrix evolves according to

$$\dot{\mathbf{R}}(t) = \mathbf{R}(t)\mathbf{S}[\boldsymbol{\omega}(t)], \tag{1}$$

where $\boldsymbol{\omega}(t) \in \mathbb{R}^3$ is the angular velocity of $\{B\}$ with respect to $\{I\}$, expressed in $\{B\}$. The measurements $\boldsymbol{\omega}_m(t) \in \mathbb{R}^3$ from the set of three high-grade, orthogonally mounted rate gyros are given by

$$\boldsymbol{\omega}_m(t) = \boldsymbol{\omega}(t) + \boldsymbol{\omega}_E(t), \tag{2}$$

where $\boldsymbol{\omega}_E(t) \in \mathbb{R}^3$ is the angular velocity of the Earth about its own axis, expressed in $\{B\}$. The body-fixed measurements of the constant inertial reference vector are denoted as $\mathbf{m}(t) \in \mathbb{R}^3$. Both $\boldsymbol{\omega}_E(t)$ and $\mathbf{m}(t)$ are constant (and known) when expressed in inertial coordinates. Hence, let ${}^I\boldsymbol{\omega}_E$ and ${}^I\mathbf{m}$ correspond to their inertial vector counterparts, such that ${}^I\boldsymbol{\omega}_E = \mathbf{R}(t)\boldsymbol{\omega}_E(t)$ and ${}^I\mathbf{m} = \mathbf{R}(t)\mathbf{m}(t)$ for all $t \geq 0$. For ease

[2] This frame is not inertial because it rotates along with the Earth. However, in practical terms, it can be considered as such because the apparent forces due to the Earth's movement are negligible.

of notation, the upper left superscripts of the body-fixed vectors were dropped, i.e., $\boldsymbol{\omega}_E \equiv {}^B\boldsymbol{\omega}_E$.

From (2), the continuous matrix differential equation (1) can be rewritten as

$$\dot{\mathbf{R}}(t) = \mathbf{R}(t)\mathbf{S}[\boldsymbol{\omega}_m(t) - \boldsymbol{\omega}_E(t)].$$

The following assumptions are considered throughout the remainder of the paper.

Assumption 1. The constant inertial vectors ${}^I\boldsymbol{\omega}_E$ and ${}^I\mathbf{m}$ are not collinear, i.e., ${}^I\boldsymbol{\omega}_E \times {}^I\mathbf{m} \neq \mathbf{0}$.

This assumption concerns observability purposes and is useful in the main result of this work. It is easily attainable in practice, since both vectors depend uniquely on the geographical location. In particular, it ensures that one can extract unequivocal information on directionality from the two vectors involved as long as they define a plane.

Assumption 2. The rate gyro measurements are bounded for all time, i.e., there exists a positive scalar $\sigma > 0$ such that, for all $t > 0$, $\|\boldsymbol{\omega}_m(t)\| \leq \sigma$.

This is a practical assumption verified across all rate gyro devices since angular velocity readings do not grow unbounded.

Consider now the following observer for the rotation matrix

$$\dot{\hat{\mathbf{R}}}(t) = \hat{\mathbf{R}}(t)\mathbf{S}\left[\boldsymbol{\omega}_m(t) - \hat{\mathbf{R}}^T(t){}^I\boldsymbol{\omega}_E + \mathbf{K}(t)\left(\mathbf{m}(t) \times \left(\hat{\mathbf{R}}^T(t){}^I\mathbf{m}\right)\right)\right], \tag{3}$$

with

$$\mathbf{K}(t) := \hat{\mathbf{R}}^T(t)\bar{\mathbf{K}}(t)\hat{\mathbf{R}}(t) \in \mathbb{R}^{3\times 3}, \tag{4}$$

where $\bar{\mathbf{K}}(t) \in \mathbb{R}^{3\times 3}$ is a continuous matrix gain to be determined. $\hat{\mathbf{R}}(t) \in SO(3)$ denotes the estimates of the rotation matrix that evolve on the manifold. Furthermore, for some $\kappa > 0$, let $\left\|\bar{\mathbf{K}}(t)\right\| \leq \kappa$, for all $t \geq 0$, therefore implying that $\mathbf{K}(t)$ is also norm-bounded by κ since, by construction, $\left\|\hat{\mathbf{R}}(t)\right\| = 1$. Define the error variable

$$\tilde{\mathbf{R}}(t) := \mathbf{R}(t)\hat{\mathbf{R}}^T(t) \in SO(3), \tag{5}$$

whose dynamics are given by

$$\begin{aligned}
\dot{\tilde{\mathbf{R}}}(t) =& \dot{\mathbf{R}}(t)\hat{\mathbf{R}}^T(t) + \mathbf{R}(t)\dot{\hat{\mathbf{R}}}^T(t)\\
=& \mathbf{R}(t)\mathbf{S}[\boldsymbol{\omega}_m(t) - \boldsymbol{\omega}_E(t)]\hat{\mathbf{R}}^T(t)\\
&+ \mathbf{R}(t)\left(\hat{\mathbf{R}}(t)\mathbf{S}\left[\boldsymbol{\omega}_m(t) - \hat{\mathbf{R}}^T(t){}^I\boldsymbol{\omega}_E + \mathbf{K}(t)\left(\mathbf{m}(t) \times \left(\hat{\mathbf{R}}^T(t){}^I\mathbf{m}\right)\right)\right]\right)^T\\
=& \mathbf{R}(t)\mathbf{S}[\boldsymbol{\omega}_m(t) - \boldsymbol{\omega}_E(t)]\hat{\mathbf{R}}^T(t)\\
&- \mathbf{R}(t)\mathbf{S}\left[\boldsymbol{\omega}_m(t) - \hat{\mathbf{R}}^T(t){}^I\boldsymbol{\omega}_E + \mathbf{K}(t)\left(\mathbf{m}(t) \times \left(\hat{\mathbf{R}}^T(t){}^I\mathbf{m}\right)\right)\right]\hat{\mathbf{R}}^T(t).
\end{aligned}$$

Isolating the terms associated with the Earth's angular velocity, and further noticing that the terms corresponding to the measurements of angular velocity cancel each other, allows to write

$$\begin{aligned}
\dot{\tilde{\mathbf{R}}}(t) =& -\mathbf{R}(t)\mathbf{S}\left[\boldsymbol{\omega}_E(t) - \hat{\mathbf{R}}^T(t){}^I\boldsymbol{\omega}_E\right]\hat{\mathbf{R}}^T(t)\\
&- \mathbf{R}(t)\mathbf{S}\left[\mathbf{K}(t)\left(\mathbf{m}(t) \times \left(\hat{\mathbf{R}}^T(t){}^I\mathbf{m}\right)\right)\right]\hat{\mathbf{R}}^T(t)\\
=& -\mathbf{R}(t)\mathbf{S}\left[\left(\mathbf{R}^T(t) - \hat{\mathbf{R}}^T(t)\right){}^I\boldsymbol{\omega}_E\right]\hat{\mathbf{R}}^T(t)\\
&- \mathbf{R}(t)\mathbf{S}\left[\mathbf{K}(t)\left(\left(\mathbf{R}^T(t){}^I\mathbf{m}\right) \times \left(\hat{\mathbf{R}}^T(t){}^I\mathbf{m}\right)\right)\right]\hat{\mathbf{R}}^T(t).
\end{aligned}$$

Since $\mathbf{R}^T(t)\mathbf{R}(t) = \mathbf{I}$, the previous result can be rewritten as

$$\begin{aligned}
\dot{\tilde{\mathbf{R}}}(t) =& -\mathbf{R}(t)\mathbf{S}\left[\left(\mathbf{R}^T(t) - \hat{\mathbf{R}}^T(t)\right){}^I\boldsymbol{\omega}_E\right]\mathbf{R}^T(t)\mathbf{R}(t)\hat{\mathbf{R}}^T(t)\\
&- \mathbf{R}(t)\mathbf{S}\left[\mathbf{K}(t)\left(\left(\mathbf{R}^T(t){}^I\mathbf{m}\right) \times \left(\hat{\mathbf{R}}^T(t){}^I\mathbf{m}\right)\right)\right]\mathbf{R}^T(t)\mathbf{R}(t)\hat{\mathbf{R}}^T(t).
\end{aligned} \tag{6}$$

Recall the error definition in (5), and employ the property

$$\mathbf{R}(t)\mathbf{S}[\mathbf{a}]\mathbf{R}^T(t) = \mathbf{S}[\mathbf{R}(t)\mathbf{a}], \quad \mathbf{a} \in \mathbb{R}^3,$$

to help simplifying (6) as

$$\begin{aligned}
\dot{\tilde{\mathbf{R}}}(t) =& -\mathbf{S}\left[\left(\mathbf{R}(t)\mathbf{R}^T(t) - \mathbf{R}(t)\hat{\mathbf{R}}^T(t)\right){}^I\boldsymbol{\omega}_E\right]\tilde{\mathbf{R}}(t)\\
&- \mathbf{S}\left[\mathbf{R}(t)\mathbf{K}(t)\left(\mathbf{R}^T(t){}^I\mathbf{m} \times \hat{\mathbf{R}}^T(t){}^I\mathbf{m}\right)\right]\tilde{\mathbf{R}}(t).
\end{aligned}$$

Finally, replace (4) in the previous equation to obtain

$$\begin{aligned}
\dot{\tilde{\mathbf{R}}}(t) =& -\mathbf{S}\left[\left(\mathbf{I} - \tilde{\mathbf{R}}(t)\right){}^I\boldsymbol{\omega}_E + \tilde{\mathbf{R}}(t)\bar{\mathbf{K}}(t)\left(\tilde{\mathbf{R}}^T(t){}^I\mathbf{m} \times {}^I\mathbf{m}\right)\right]\tilde{\mathbf{R}}(t)\\
=& \tilde{\mathbf{R}}(t)\mathbf{S}\left[\left(\mathbf{I} - \tilde{\mathbf{R}}^T(t)\right){}^I\boldsymbol{\omega}_E - \bar{\mathbf{K}}(t)\left(\tilde{\mathbf{R}}^T(t){}^I\mathbf{m} \times {}^I\mathbf{m}\right)\right].
\end{aligned} \tag{7}$$

This last result poses a highly nonlinear relationship, whereby classical tools from linear system theory cannot be applied. But before moving on to the stability analysis of the nonlinear error dynamics (7), one must find a suitable matrix gain $\bar{\mathbf{K}}(t)$ to drive the estimation error to zero, i.e., to asymptotically drive the error matrix $\tilde{\mathbf{R}}(t)$ to an identity, as suggested by (5).

3. Computation of observer gain $\bar{\mathbf{K}}(t)$

3.1. Local stability analysis

A simple strategy is proposed to determine $\bar{\mathbf{K}}(t)$. It is based on previous work by the authors, see Reis et al. (2019), and arises from considering only small perturbations of the rotation matrix.

First, let $\boldsymbol{\theta}(t) \in \mathbb{R}^3$ denote the Euler angles associated with $\mathbf{R}(t)$ and let $\mathbf{u} \in \mathbb{R}^3$ be a constant arbitrary vector. Second, consider the estimated rotation matrix $\hat{\mathbf{R}}(t)$ as the result of a slight perturbation over the nominal rotation matrix, and regard it as a parameterization of $\mathbf{R}(t)$ in terms of the nominal Euler angles $\bar{\boldsymbol{\theta}}(t)$ and of an infinitesimal deviation denoted by $\delta\boldsymbol{\theta}(t)$. Hence, the Taylor-series expansion of $\hat{\mathbf{R}}(t)\mathbf{u} = \mathbf{R}\left(\bar{\boldsymbol{\theta}}(t) + \delta\boldsymbol{\theta}(t)\right)\mathbf{u}$ can be written as

$$\hat{\mathbf{R}}(t)\mathbf{u} = \mathbf{R}\left(\bar{\boldsymbol{\theta}}(t)\right)\mathbf{u} + \left.\frac{\partial\left(\mathbf{R}\left(\boldsymbol{\theta}\right)\mathbf{u}\right)}{\partial\boldsymbol{\theta}}\right|_{\bar{\boldsymbol{\theta}}(t)}\delta\boldsymbol{\theta}(t) + \text{h.o.t},$$

which, after applying a first order approximation, results in (vide (Barfoot, Forbes, & Furgale, 2011))

$$\hat{\mathbf{R}}(t) \approx \left(\mathbf{I} - \mathbf{S}\left[\mathbf{M}\left(\bar{\boldsymbol{\theta}}(t)\right)\delta\boldsymbol{\theta}(t)\right]\right)\mathbf{R}(t), \tag{8}$$

where, for ease of notation, $\mathbf{R}(t) \equiv \mathbf{R}\left(\bar{\boldsymbol{\theta}}(t)\right)$. $\mathbf{M}\left(\bar{\boldsymbol{\theta}}(t)\right) \in \mathbb{R}^{3\times 3}$ is the linear mapping between Euler-angle rates and angular velocity $\boldsymbol{\omega}$. This result could have also been derived from the well-known Rodrigues' rotation formula. Therefore, according to (5), it follows from (8) that

$$\tilde{\mathbf{R}}(t) \approx \mathbf{I} + \mathbf{S}[\mathbf{x}(t)], \tag{9}$$

where $\mathbf{x}(t) := \mathbf{M}\left(\bar{\boldsymbol{\theta}}(t)\right)\delta\boldsymbol{\theta}(t) \in \mathbb{R}^3$. This vector can be interpreted as a pseudo rotation vector whose components correspond to infinitesimal amounts of rotations about the three axis of the reference frame.

According to the previous linearization expressed by (9), substitute in (7) all terms denoted by $\tilde{\mathbf{R}}(t)$ and simplify in order to get

$$\begin{aligned}
\dot{\tilde{\mathbf{R}}}(t) \approx& \left(\mathbf{I} + \mathbf{S}[\mathbf{x}(t)]\right)\mathbf{S}\left[\mathbf{S}[\mathbf{x}(t)]{}^I\boldsymbol{\omega}_E + \bar{\mathbf{K}}(t)\left(\left(\mathbf{S}[\mathbf{x}(t)]{}^I\mathbf{m}\right) \times {}^I\mathbf{m}\right)\right]\\
=& \left(\mathbf{I} + \mathbf{S}[\mathbf{x}(t)]\right)\mathbf{S}\left[-\mathbf{S}\left[{}^I\boldsymbol{\omega}_E\right]\mathbf{x}(t) + \bar{\mathbf{K}}(t)\mathbf{S}^2\left[{}^I\mathbf{m}\right]\mathbf{x}(t)\right].
\end{aligned}$$

Neglecting once more all second-order terms results in

$$\dot{\tilde{\mathbf{R}}}(t) \approx -\mathbf{S}\left[\mathbf{S}\left[{}^I\boldsymbol{\omega}_E\right]\mathbf{x}(t) - \bar{\mathbf{K}}(t)\mathbf{S}^2\left[{}^I\mathbf{m}\right]\mathbf{x}(t)\right],$$

which, by comparison with $\dot{\tilde{\mathbf{R}}}(t) \approx \mathbf{S}\left[\dot{\mathbf{x}}(t)\right]$, as suggested by (9), allows to write the linear differential equation

$$\dot{\mathbf{x}}(t) = \mathbf{A}(t)\mathbf{x}(t), \tag{10}$$

where $\mathbf{A}(t) := -\mathbf{S}\left[{}^I\boldsymbol{\omega}_E\right] + \bar{\mathbf{K}}(t)\mathbf{S}^2\left[{}^I\mathbf{m}\right]$.

The key target will now consist in determining $\bar{\mathbf{K}}(t)$ such that (10) converges globally exponentially fast to zero. If $\bar{\mathbf{K}}(t)$ were constant, it would suffice to make $\mathbf{A}(t) \equiv \mathbf{A}$ Hurwitz, i.e., to ensure that the real part of all eigenvalues of $\mathbf{A}$ is negative, which can be attained if the pair $\left(\mathbf{S}\left[{}^I\boldsymbol{\omega}_E\right], \mathbf{S}^2\left[{}^I\mathbf{m}\right]\right)$ is observable. However, since stability criteria of linear time-invariant (LTI) systems do not apply to linear time-varying

(LTV) systems, one must attempt a different approach, in particular by taking advantage of the Luenberger-like structure of the matrix $\mathbf{A}(t)$. Indeed, the differential equation (10) can be regarded as the dynamics of a state estimation error corresponding to an auxiliary system where $\bar{\mathbf{K}}(t)$ multiplies a feedback term on a pseudo estimation error. The reader familiar with the design of state observers immediately understands that $\bar{\mathbf{K}}(t)$ is optimal (in the sense that minimizes the variance of the pseudo estimation error) when associated with a Kalman filter.

Further details on the structure of this auxiliary system, as well as on the computation of $\bar{\mathbf{K}}(t)$, are presented in the sequel.

3.2. Kalman filter application

Consider the following continuous-time LTI system

$$\begin{cases} \dot{\boldsymbol{x}}(t) = \boldsymbol{\mathcal{A}}\boldsymbol{x}(t) + \boldsymbol{w}(t) \\ \boldsymbol{y}(t) = \boldsymbol{C}\boldsymbol{x}(t) + \boldsymbol{v}(t), \end{cases} \tag{11}$$

where $\boldsymbol{x}(t) \in \mathbb{R}^3$ represents the state vector, $\boldsymbol{y}(t) \in \mathbb{R}^3$ is the observations vector, and where $\boldsymbol{\mathcal{A}} = -\mathbf{S}\left[{}^I\boldsymbol{\omega}_E\right]$ and $\boldsymbol{C} = -\mathbf{S}^2\left[{}^I\mathbf{m}\right]$ are the dynamics and observations matrices, respectively. Let $\boldsymbol{w}(t)$ and $\boldsymbol{v}(t)$ denote additive white Gaussian noise sequences associated with the process and the measurements, respectively, such that $\boldsymbol{w}(t) \sim \mathcal{N}(\mathbf{0}, \boldsymbol{\mathcal{Q}})$ and $\boldsymbol{v}(t) \sim \mathcal{N}(\mathbf{0}, \boldsymbol{\mathcal{R}})$. $\boldsymbol{\mathcal{Q}} \in \mathbb{R}^{3\times3}$ and $\boldsymbol{\mathcal{R}} \in \mathbb{R}^{3\times3}$ are both assumed constant, symmetric, bounded, positive definite covariance matrices, each corresponding to a zero mean multivariate normal distribution.

Lemma 1. *Under Assumption 1, the continuous-time LTI system (11) is observable.*

Proof. The continuous-time LTI system (11) is observable if and only if the observability matrix $\boldsymbol{\mathcal{O}} \in \mathbb{R}^{9\times3}$ associated with the pair $(\boldsymbol{\mathcal{A}}, \boldsymbol{C})$ is full rank (rank = 3), with

$$\boldsymbol{\mathcal{O}} = \begin{bmatrix} \boldsymbol{C} \\ \boldsymbol{C}\boldsymbol{\mathcal{A}} \\ \boldsymbol{C}\boldsymbol{\mathcal{A}}^2 \end{bmatrix} = \begin{bmatrix} -\mathbf{S}^2\left[{}^I\mathbf{m}\right] \\ \mathbf{S}^2\left[{}^I\mathbf{m}\right]\mathbf{S}\left[{}^I\boldsymbol{\omega}_E\right] \\ -\mathbf{S}^2\left[{}^I\mathbf{m}\right]\mathbf{S}^2\left[{}^I\boldsymbol{\omega}_E\right] \end{bmatrix}.$$

By contradiction, suppose that Assumption 1 holds and that the LTI system (11) is not observable. This implication corresponds to the matrix $\boldsymbol{\mathcal{O}}$ not being full rank, which means $\boldsymbol{\mathcal{O}}\mathbf{v} = \mathbf{0}$, for some unit vector $\mathbf{v} \in \mathbb{R}^3$, with $\|\mathbf{v}\| = 1$. From $-\mathbf{S}^2\left[{}^I\mathbf{m}\right]\mathbf{v} = \mathbf{0}$ it follows that $\mathbf{v} = \pm{}^I\mathbf{m}/\|{}^I\mathbf{m}\|$. In turn, $\mathbf{S}^2\left[{}^I\mathbf{m}\right]\mathbf{S}\left[{}^I\boldsymbol{\omega}_E\right]\mathbf{v} = \mathbf{0}$ implies either that $\mathbf{v} = \pm{}^I\boldsymbol{\omega}_E/\|{}^I\boldsymbol{\omega}_E\|$ or that ${}^I\boldsymbol{\omega}_E \times \mathbf{v} = \pm{}^I\mathbf{m}$. However, since, according to Assumption 1, ${}^I\boldsymbol{\omega}_E$ is not collinear with ${}^I\mathbf{m}$, the only possible solution of $\boldsymbol{\mathcal{O}}\mathbf{v} = \mathbf{0}$ is $\mathbf{v} = \mathbf{0}$, but that contradicts the claim whereby $\mathbf{v}$ is a unit vector. Therefore, $\boldsymbol{\mathcal{O}}$ is always full rank and the LTI system (11) is observable. □

A classic continuous-time Kalman filter follows as the natural estimation solution for the LTI system (11). The design of the filter is omitted as it is widely-known. Hence, let $\hat{\boldsymbol{x}}(t)$ denote the filter estimates of $\boldsymbol{x}(t)$. Accordingly, the dynamics of $\hat{\boldsymbol{x}}(t)$ are governed by

$$\dot{\hat{\boldsymbol{x}}}(t) = \boldsymbol{\mathcal{A}}\hat{\boldsymbol{x}}(t) + \bar{\mathbf{K}}(t)\left(\boldsymbol{y}(t) - \boldsymbol{C}\hat{\boldsymbol{x}}(t)\right). \tag{12}$$

Define now the error variable $\boldsymbol{e}(t) := \boldsymbol{x}(t) - \hat{\boldsymbol{x}}(t)$. From (11) and (12), one concludes that the nominal error dynamics obey

$$\dot{\boldsymbol{e}}(t) = \left(\boldsymbol{\mathcal{A}} - \bar{\mathbf{K}}(t)\boldsymbol{C}\right)\boldsymbol{e}(t), \tag{13}$$

which has a direct correspondence to (10). In turn, the computation of the matrix gain $\bar{\mathbf{K}}(t)$ stems inherently from the solution of the Riccati differential matrix equation,

$$\dot{\mathbf{P}}(t) = -\mathbf{P}(t)\boldsymbol{C}^T\boldsymbol{\mathcal{R}}^{-1}\boldsymbol{C}\mathbf{P}(t) + \boldsymbol{\mathcal{A}}\mathbf{P}(t) + \mathbf{P}(t)\boldsymbol{\mathcal{A}}^T + \boldsymbol{\mathcal{Q}}, \tag{14}$$

with $\mathbf{P}(t = t_0) = \mathbf{P}_0 \succ \mathbf{0}$, and is thus given by

$$\bar{\mathbf{K}}(t) = \mathbf{P}(t)\boldsymbol{C}^T\boldsymbol{\mathcal{R}}^{-1}. \tag{15}$$

According to Rugh (1996, Definition 18.30), the LTI system is detectable because (13) is exponentially stable. Nevertheless, on account of the pair $(\boldsymbol{\mathcal{A}}, \boldsymbol{C})$ being observable, the same conclusion could have been inferred because detectability is a weaker condition than observability. If a system is observable, then it is also detectable and, therefore, according to Kučera (1973, Theorem 8), the solution of the Riccati equation (14) is bounded for all time, which complies with the established assumption that $\|\bar{\mathbf{K}}(t)\| \leq \kappa$, for some $\kappa > 0$. With $\mathbf{P}(t)$ bounded, it follows from (14) that $\dot{\mathbf{P}}(t)$ is also bounded.

Remark 1. The Kalman gain, as given by (15), will be employed in the nonlinear observer (3). An obvious advantage of this implementation is that one simply has to tune the matrices $\boldsymbol{\mathcal{Q}} \succ \mathbf{0}$ and $\boldsymbol{\mathcal{R}} \succ \mathbf{0}$ while guided by a paramount insight provided by the LTI system (11). Most noticeably, on account of the system being observable, the error term $\boldsymbol{e}(t)$, i.e., $\mathbf{x}(t)$ as given by (10), is guaranteed to converge globally exponentially fast to zero, which, at this stage, automatically renders the proposed nonlinear observer (3) locally exponentially stable (Khalil, 2002, Theorem 4.13).

4. Performance analysis

In this section, several simulation tests will be conducted, including Monte Carlo runs. After a rigorous description of a realistic simulation setup, the first set of simulations will validate the efficiency of the proposed attitude estimation solution in terms of its local performance, for which exponential stability has been ensured. Then, in order to understand the range of applicability of the nonlinear observer (3) in the absence of global asymptotic stability guarantees, additional tests will take into account a set of admissible initial conditions uniformly distributed in $SO(3)$, whereby Monte Carlo runs will help assessing the repeatability of the system's behavior.

Consider henceforward the general parameterization of the rotation matrix error by means of a unit vector (axis of rotation) $\tilde{\mathbf{v}}(t)$ and an angle $\tilde{\theta}(t) \in [0,\ \pi]$. This formalism, also known as Euler angle-axis representation, is expressed by

$$\tilde{\mathbf{R}}(t) = \mathbf{I} + \sin\left(\tilde{\theta}(t)\right)\mathbf{S}\left[\tilde{\mathbf{v}}(t)\right] + \left[1 - \cos\left(\tilde{\theta}(t)\right)\right]\mathbf{S}^2\left[\tilde{\mathbf{v}}(t)\right] \tag{16}$$

and proves very useful in the error analysis of observers that are built on $SO(3)$.

4.1. Simulation setup

Consider a robotic platform describing a three-dimensional rotational motion, located at a latitude of $\varphi = 38.777816°$ North, a longitude of $\psi = 9.097570°$ West, and at sea level. Taking into account the period of time known as sidereal day, the corresponding norm of the Earth's angular velocity is $\left\|{}^I\boldsymbol{\omega}_E\right\| = 7.2921159 \times 10^{-5}$ rad/s (approximately 15 degrees per hour), whose vectorial representation in the local NED frame is given by ${}^I\boldsymbol{\omega}_E = \left\|{}^I\boldsymbol{\omega}_E\right\|[\cos(\varphi)\ 0\ \sin(\varphi)]^T$ rad/s. Moreover, in light of the sea level and of the latitude indicated above, according to the International Gravity Formula 1980, the components of the inertial acceleration due to gravity are given by

$${}^I\mathbf{m} = [0\ 0\ 9.800611]^T\ \ \mathrm{m/s^2}.$$

One easily verifies that ${}^I\boldsymbol{\omega}_E \times {}^I\mathbf{m} = [0\ \ -0.5571 \times 10^{-3}\ \ 0]^T$ (rad·m/s^3), which satisfies Assumption 1. Further suppose that the body-vector measurements of the acceleration of gravity are collected by the 3-axis accelerometer embedded in the commercial off-the-shelf 1775 FOG IMU from KVH Industries. In order to emulate this unit's accelerometers worst case specifications, which are characterized by a Velocity Random Walk of 0.12 mg/$\sqrt{\mathrm{Hz}}$, a zero-mean white Gaussian noise sequence with standard deviation of 0.0059 m/s^2 was added over the accelerometer measurements across all simulations, assuming

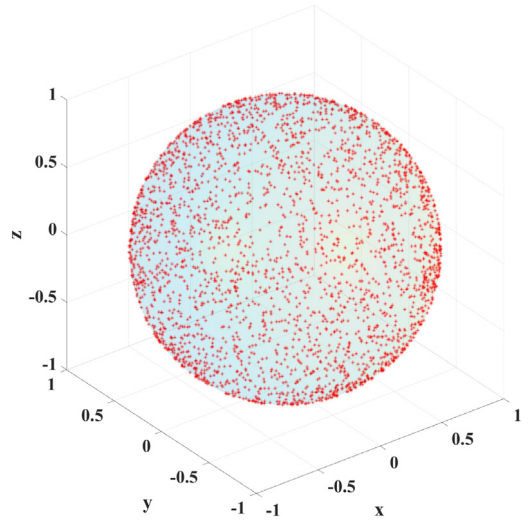

Fig. 1. Initial axes of rotation on the unit sphere (local evaluation).

a sampling frequency of 25 Hz. The angular velocity of the platform, expressed on the body frame, was designed as follows:

$$\boldsymbol{\omega}(t) = \left[5\sin\left(\frac{6\pi}{180}\right) \quad \sin\left(\frac{\pi}{180}t\right) \quad -2\sin\left(\frac{6}{5}\frac{\pi}{180}t\right)\right]^T \quad \text{(deg/s)}.$$

The initial attitude of the platform was always set to $\mathbf{R}(0) = \mathbf{I}$.

Regarding the angular velocity readings, they were assumed to be collected from the high-grade rate gyros also embedded in the 1775 Fiber Optic Gyro IMU. According to the manufacturer, with digital output the rate gyro measurements are corrupted by an Angle Random Walk (ARW) noise of $0.7°/\text{hr}/\sqrt{\text{Hz}}$, which was taken into account in the simulations. Once again, for a sampling frequency of 25 Hz, and given a rate-integrating configuration, this ARW noise translates roughly into a standard deviation of 0.972 millidegrees per second.

4.2. Local dynamic behavior evaluation

The first order approximation of $\tilde{\mathbf{R}}(t)$, given by (9), is often regarded as the small angles approximation of the rotation matrix error, which stems from (16) by setting $\sin(\tilde{\theta}(t)) \approx \tilde{\theta}(t)$ and $\cos(\tilde{\theta}(t)) \approx 1$. In order to remain below 1% in terms of relative error of the small angles approximation, this local evaluation should abide by initial conditions where $\tilde{\theta}(t=0) < 14$ degrees. Hence, resorting to the Monte Carlo method, 100 runs were performed for every initial angle error $\tilde{\theta}(t=0)$ in the interval $\{0.5, 1, 1.5, \ldots, 14\}$ (degrees). Each Monte Carlo run features randomly generated noise sequences and initial axes of rotation. Fig. 1 illustrates the nicely covered unit sphere containing all axes $\tilde{\mathbf{v}}(t=0)$ associated with the total $28 \cdot 100$ Monte Carlo runs.

Regarding the simulation parameters, the covariance matrices of the filter were adjusted empirically for the best achievable results. More specifically, the covariance of the process noise was set to $\boldsymbol{\mathcal{Q}} = 5\times10^{-9}\mathbf{I}$; the covariance of the observations noise was set to $\boldsymbol{\mathcal{R}} = 10^{-2}\mathbf{I}$; and, a large initial covariance estimate of $\mathbf{P}(0) = 0.05\mathbf{I}$ was used to ensure fast convergence. The evolution of $\tilde{\theta}(t)$ for each of the 28 initial conditions is shown in Fig. 2, where it is possible to immediately infer an obvious consistency between initial deviation and convergence time. Meanwhile, in steady-state, all errors remain below 0.4 degrees after just 10 minutes, which corresponds to a very good performance in the presence of realistic sensor noise.

Furthermore, there is an almost unnoticeable swift convergence that takes place during the first few sampling instants. The initial deviation, despite spanning angles between 0.5 and 14 degrees, seems to never surpass 8 degrees. This a consequence of the time-varying nature of the observer gain, which is inherently interconnected with the solution of

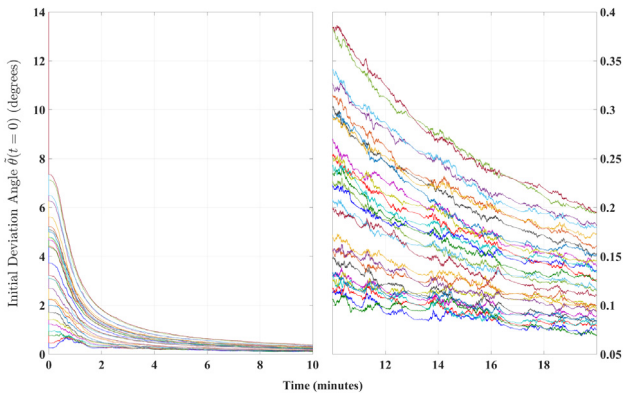

Fig. 2. Time evolution of $\tilde{\theta}(t)$ for $\tilde{\theta}(0) = 0.5 \ldots 14$ degrees (local evaluation).

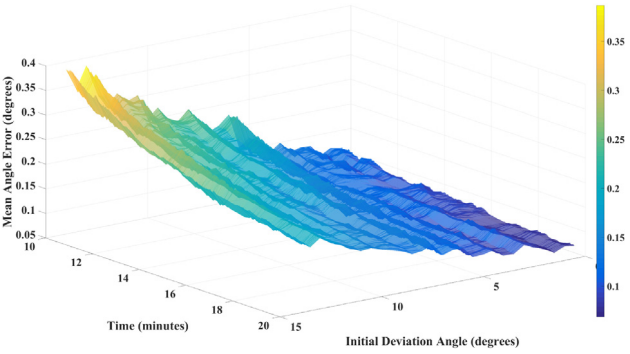

Fig. 3. Steady state mean of $\tilde{\theta}(t)$ for $t \geq 10$ minutes (local evaluation).

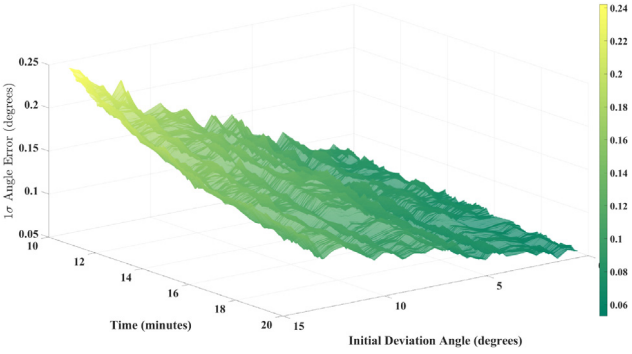

Fig. 4. Steady state standard deviation of $\tilde{\theta}(t)$ for $t \geq 10$ minutes (local evaluation).

the Riccati equation (14). That solution also displays a rapid transition resulting from the choice of gains and, as shown in the next section, its time-varying nature is of the utmost importance for attaining the fastest achievable performance.

The mean and standard deviation values were also computed and averaged for each set of 100 runs. The results are depicted in Figs. 3 and 4, respectively. The growth pattern of both accumulated values is consistent with the initial deviation and displays a decreasing trend.

4.3. On the attainable performance considering $\dot{\mathbf{P}}(t) = 0$

In many practical applications to reduce the computational burden associated to the Riccati equation, it is common to resort to the algebraic solution $\mathbf{P}$ of

$$\mathbf{0} = -\mathbf{P}\boldsymbol{\mathcal{C}}^T\boldsymbol{\mathcal{R}}^{-1}\boldsymbol{\mathcal{C}}\mathbf{P} + \boldsymbol{\mathcal{A}}\mathbf{P} + \mathbf{P}\boldsymbol{\mathcal{A}}^T + \boldsymbol{\mathcal{Q}}. \tag{17}$$

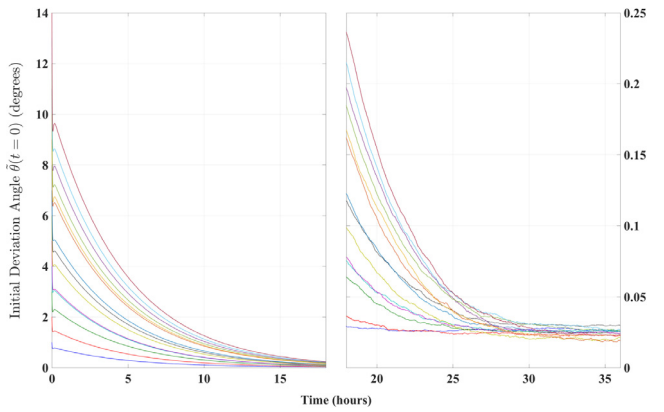

Fig. 5. Time evolution of $\tilde{\theta}(t)$ for $\tilde{\theta}(0) = 1, 2 \dots 14$ degrees (local evaluation with $\dot{\mathbf{P}}(t) = \mathbf{0}$).

This solution, under similar conditions, guarantees a stable filter behavior. Nevertheless, due to its simplicity and low computational power requirements, it is relevant to investigate how the nature of this solution can impact the performance of the proposed observer. In other words, can the steady state matrix $\mathbf{P}$, solution of (17), attain similar performance as its time-varying counterpart, which results from solving (14)? The answer, in the absence of analytic expressions, will have to resort exclusively to simulation results. Therefore, a similar Monte Carlo analysis will be implemented, only this time using a steady-state matrix $\mathbf{P}$, which can be easily computed from (17) by resorting to the MATLAB function `care`$(\boldsymbol{\mathcal{A}}^T, \boldsymbol{\mathcal{C}}^T, \boldsymbol{\mathcal{Q}}, \boldsymbol{\mathcal{R}}, \mathbf{0}, \mathbf{I})$.[3] The covariance of the observations noise was set empirically to $\boldsymbol{\mathcal{R}} = 10^{-4}\mathbf{I}$ for an overall best performance. The final results are shown in Fig. 5, which contains the error evolution of 14 sequences, each corresponding to an initial angle deviation $\tilde{\theta}(0)$ in the interval $\{1, 2 \dots 14\}$ (degrees). The overall convergence behavior is indeed quite similar to the one displayed in Fig. 2, although convergence times are now extremely slow, taking approximately 24 h for the filter to reach steady-state. This was a somewhat expected result, in line with the performance of the nonlinear observer proposed by the authors in Reis et al. (2019). When the Kalman filter gain is assumed constant, the performance of the observer is essentially dictated by the fixed eigenvalues of the matrix $\mathbf{A}$, as shown in (10). Furthermore, without the time-varying nature of its gain, the Kalman filter is, to some extent, limited to the directionality of both vectors ${}^I\boldsymbol{\omega}_E$ and ${}^I\mathbf{m}$. Notice, either from (10) or (13), how the former vector is not even affected by the gain, which hints towards a much more intricate role of $\mathbf{P}(t)$ in the observer performance.

4.4. Observer performance beyond local restrictions

Although the time varying filtering solution, with feedback gain $\bar{\mathbf{K}}(t)$ provided by the Kalman filter, stabilizes the linear error dynamics (13), care must be taken when extrapolating these statements from $\mathbb{R}^3$ to $SO(3)$, where, by definition, $\|\mathbf{x}(t)\| \leq 1$ for all $t \geq 0$.

In the previous section, it was shown that the time-varying nature of the Kalman gain remarkably improves the local performance of the proposed observer, reducing convergence times from several hours down to a few minutes. What remains to check is whether the attitude observer (3) behaves well for initial deviations up to $\tilde{\theta}(t = 0) < 180$ degrees. To assess that, a new Monte Carlo analysis will be conducted, consisting basically in an extension of the one carried out in Section 4.2. Only the initial covariance of the error was updated to $\mathbf{P}(0) = 5\mathbf{I}$ to ensure a fast initial transient for all error sequences.

[3] This function computes the unique solution of the continuous-time algebraic Riccati equation.

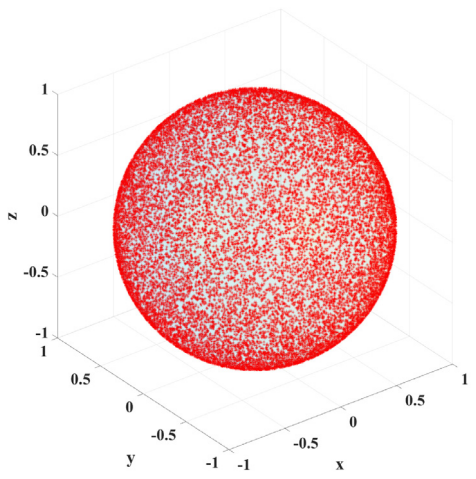

Fig. 6. Initial axes of rotation on the unit sphere.

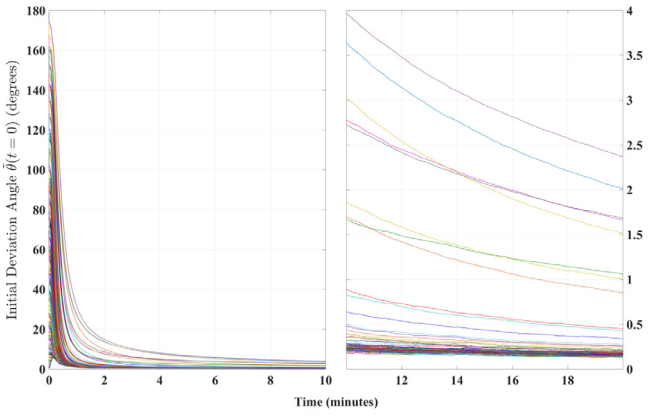

Fig. 7. Time evolution of $\tilde{\theta}(t)$ for $\tilde{\theta}(0) = 1, 2, \dots, 179$ degrees.

Fig. 6 illustrates the practically covered unit sphere containing all initial axes of rotation $\bar{\mathbf{v}}(t = 0)$, which, along with the interval of initial angle deviations, helps corroborating the claim that the proposed nonlinear observer works, under the established assumptions, for a large basin of attraction. This claim is further validated by the results displayed in Fig. 7, which shows, for each $\tilde{\theta}(t = 0) \in [1, 179]$, the averaged evolution of the corresponding 100 Monte Carlo runs. The initial transient is roughly under 2 min for all sequences, with convergence times being function of the initial deviation, as expected.

Going into more detail, Figs. 8 and 9 exhibit the steady-state behavior of both the averaged mean and averaged standard deviation, for $t \geq 10$ minutes, as a function of $\tilde{\theta}(t)$. The two plots hint the performance level that can be attained by the proposed filter, with means and standard deviations consistently lower than 0.25 and 0.2 degrees, respectively. This level of accuracy, together with fast convergence rates, deems the proposed nonlinear observer a suitable choice across many application scenarios, for example, in space applications and submarine operations.

As a side note, it is important to remark that the nature of sensor noise is not obvious when dealing with experiments. Still, Gaussian noises are quite common across most robotic applications, which in turn motivated the simulation setup presented in this work. Nevertheless, a second extensive Monte Carlo analysis was carried out considering uniform noise. The uniform distribution of random samples, corresponding to noise over sensor measurements, was set to range in the interval $[-3\sigma, 3\sigma]$, with σ being the standard deviation of the Gaussian distributions which characterize the sensors employed.

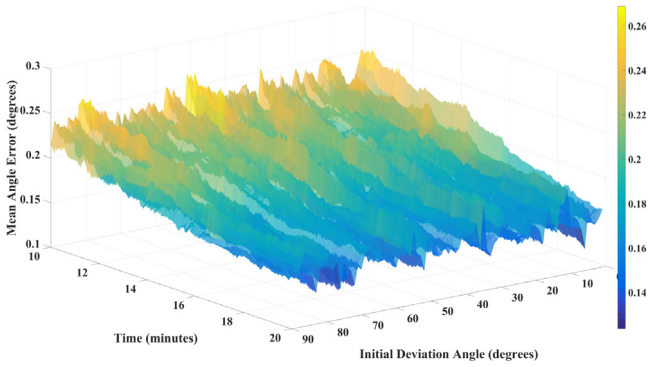

Fig. 8. Steady state mean of $\tilde{\theta}(t)$ for $t \geq 10$ minutes.

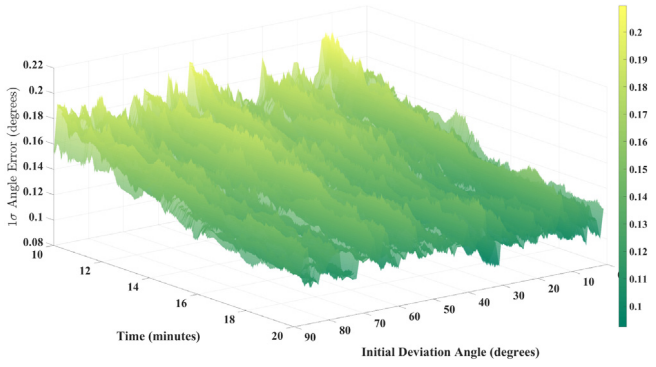

Fig. 9. Steady state standard deviation of $\tilde{\theta}(t)$ for $t \geq 10$ minutes.

Overall, the resulting performance is very similar to the one attained in the Gaussian case, both in terms of convergence time and steady-state accuracy.

5. Experimental results

In order to validate the nonlinear observer (3), an experiment was carried out using a tri-axial high-grade FOG IMU KVH® 1775 mounted on a Ideal Aerosmith Model 2103HT Three-Axis Positioning and Motion Rate Table (MRT), which is designed to provide precise position, rate, and acceleration motion, for instance, for the development and/or production testing and calibration of IMUs and Inertial Navigation Systems. The ground-truth data from the MRT is characterized by a rate accuracy of $0.5\% \pm 0.0005$ deg/sec on its limited rotation axes (y and z) and $0.01\% \pm 0.0005$ deg/sec on its unlimited rotation axis (x), and by a position accuracy of 30 arc sec on all axes. The final experimental setup, whose location in terms of Earth coordinates is approximately the same as indicated in the beginning of Section 4.1, is depicted in Fig. 10.

The FOG IMU provides tri-axial angular velocity, acceleration and magnetometer readings. However, due to the unreliability of the tri-axial magnetometer, which, in this particular case, is greatly affected by hard- and soft-iron effects caused by the MRT, as well as by the magnetic fields generated by the electric motors, this sensor was discarded. Instead, we resorted to accelerometer measurements by considering slow rotational maneuvers to ensure that the magnitude of the gravitational field is the dominant acceleration term. At room temperature, this FOG IMU's accelerometer is characterized by a velocity random walk of $0.12\ \text{mg}/\sqrt{\text{Hz}}$, which corresponds to the same noise considered in the simulations.

It is worth mentioning that the nature of the KVH FOG 1775 precludes the existence of outliers, which are exceptionally rare in high-grade sensors. Detecting and removing inconsistent observations

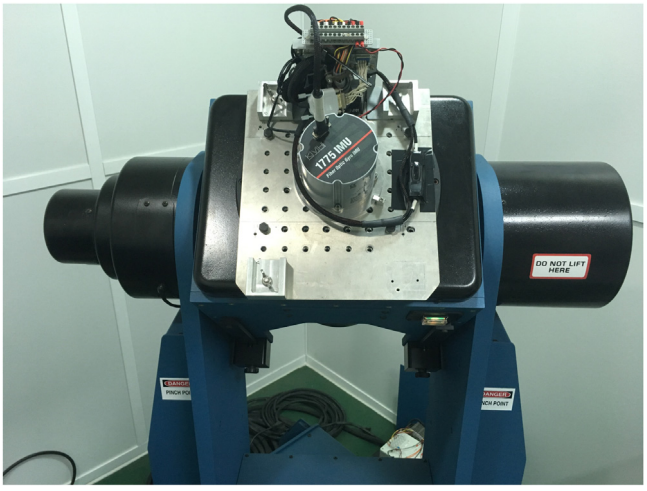

Fig. 10. Experimental setup.

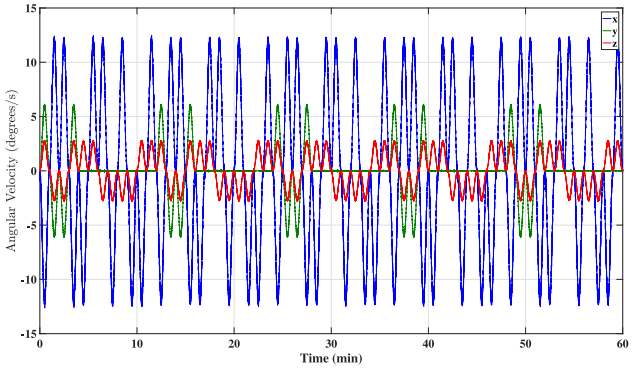

Fig. 11. MRT angular velocity on body-frame.

remain nevertheless active research fields, drawing a lot of attention from the scientific community, but they are both out of the scope of this work. An in-depth look at this issue, specially in the case when measurements have non-Gaussian distributions, can be found in, e.g., Stojanovic and Nedic (2015) and references therein.

A calibration procedure was implemented beforehand that determined a matrix of constant scaling factors, a constant bias and a corresponding inertial vector (with respect to the MRT's own local NED inertial frame), for both the rate gyro and accelerometer. Data acquired from the MRT was sampled at 128 Hz, and later down-sampled to 25 Hz to match the sampling frequency of the FOG IMU.

Fig. 11 shows the ground-truth data corresponding to the angular velocity of the MRT, as expressed on its reference frame. The rotational motion lasted approximately one hour. The data was then fed to the nonlinear attitude observer (3), which was run 100 times, each iteration using a randomly generated initial rotation matrix estimate, computed as the exponential matrix of a random vector. The spacial distribution of the resulting axes of rotation associated with the 100 estimates is depicted in Fig. 12. For the sake of completeness, the 100 initial angle errors corresponding to the randomly generated rotation matrices are shown, sorted in increasing order, in Fig. 13.

The plot with the final attitude estimation results, which consist in an average over time of the 100 observer iterations, is displayed in Fig. 14. The convergence can be seen to reach steady-state after around 10 min, following an unconventional transient characterized by somewhat large oscillations. We recall that the role of $\mathbf{P}(t)$ in the observer remains partly unknown; the only certainty is that $\mathbf{P}(t)$ indeed converges asymptotically to a positive-definite symmetric matrix,

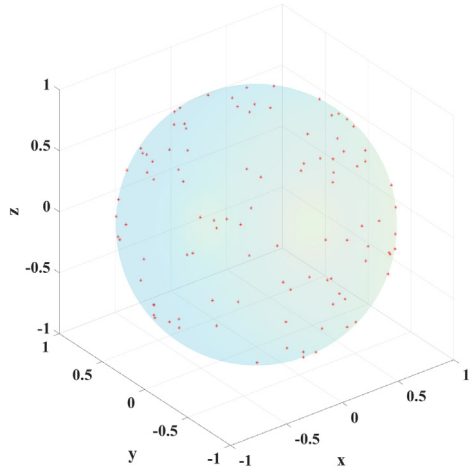

Fig. 12. Initial axes of rotation on the sphere. (Experimental Evaluation).

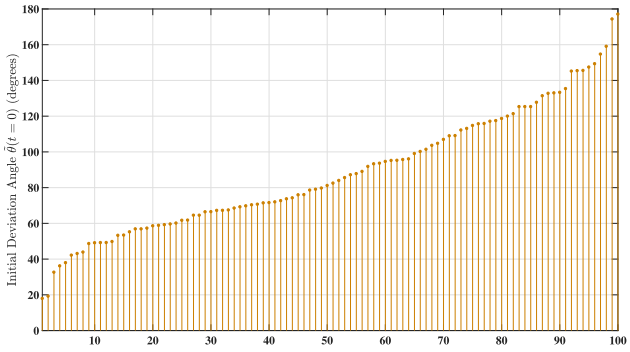

Fig. 13. Initial angle deviations. (Experimental Evaluation).

Table 1
Summary of results: averaged mean (μ) and standard deviation (σ) of all angle error sequences, for $t \geq 30$ min.

Measure	Simulation	Experimental
μ (degrees)	0.1408	0.4664
σ (degrees)	0.2619	0.2561

which can actually be computed a priori. Convergence of the solution of the Riccati differential equation (14) to the algebraic Riccati equation solution, for LTI systems, has been studied before, with several results found in the literature. The reader is referred to, for instance, Bitmead and Gevers (1991, Theorem 10.10). Moreover, $\mathbf{P}(t)$ is independent of the trajectory described by the MRT, which means it can be computed offline. Most noticeably, the averaged angle error remains most of the time below 1 degree, with mean and standard deviation, computed for $t \geq 30$ min, equal to 0.4664 and 0.2561 degrees, respectively. These experimental results, which compare fairly similar to the ones obtained in simulation, as seen from Table 1, confirm the performance of the proposed solution, which can be used in many ocean, air, and ground robotic applications, even when accounting for changes in geographical location, i.e., translational motion, since the reference vector variation is only slightly affected. Indeed, at the surface of the planet, a 100 km displacement corresponds roughly to covering a 1 degree arc length.

6. Conclusions

In this paper, a nonlinear attitude observer built on $SO(3)$ was proposed that takes into account the Earth's rotational velocity and resorts exclusively to single body measurements of a constant inertial reference vector, in addition to angular velocity readings. In view of the highly nonlinear structure of the attitude error dynamics, a linearization was carried out that resulted in the establishment of an LTV system. This LTV system was in turn shown to have a direct correspondence to an LTV Luenberger observer for an LTI system, which was proved to be observable. A Kalman filter followed as the natural estimation solution, rendering the nonlinear observer locally exponentially stable. Extensive simulation and experimental results have allowed to assess the performance of the observer to a great extent. Indeed, the error associated to the nonlinear attitude observer converges to zero for all initial conditions up to the critical angle deviation of 180 degrees, therefore demonstrating the applicability of the proposed nonlinear attitude in real world ocean, air and ground vehicular applications.

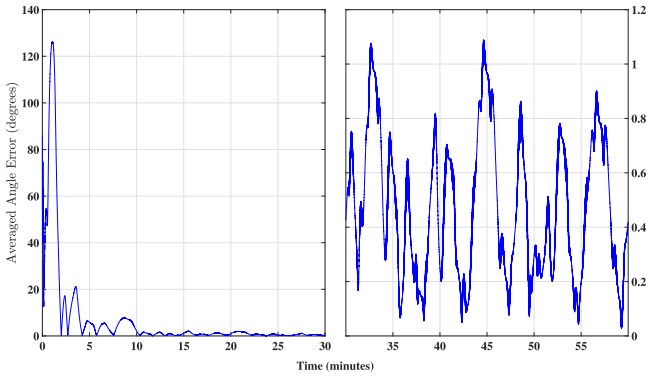

Fig. 14. Averaged angle error evolution.

Declaration of competing interest

The authors declare that they have no known competing financial interests or personal relationships that could have appeared to influence the work reported in this paper.

Acknowledgments

This work was supported by the Macao Science and Technology Development Fund under Grant FDCT/026/2017/A1, by the University of Macau, Macao, China, under Project MYRG2018-00198-FST and by the Portuguese Fundação para a Ciência e a Tecnologia (FCT) through Institute for Systems and Robotics (ISR), under Laboratory for Robotics and Engineering Systems (LARSyS) [UID/EEA/50009/2013] and through Institute for Mechanical Engineering (IDMEC), under Associated Laboratory for Energy, Transports and Aeronautics (LAETA) [UID/EMS/50022/2013] projects, and through the FCT project DECENTER [LISBOA-01-0145-FEDER-029605], funded by the Lisboa 2020 and PIDDAC programs.

References

Bachmann, E. R., Yun, X., & Brumfield, A. (2007). Limitations of attitude estimnation algorithms for inertial/magnetic sensor modules. *IEEE Robotics & Automation Magazine*, *14*(3), 76–87.

Barfoot, T., Forbes, J. R., & Furgale, P. T. (2011). Pose estimation using linearized rotations and quaternion algebra. *Acta Astronautica*, *68*(1–2), 101–112.

Barrau, A., & Bonnabel, S. (2017). The invariant extended kalman filter as a stable observer. *IEEE Transactions on Automatic Control*, *62*(4), 1797–1812.

Batista, P., Silvestre, C., & Oliveira, P. (2012). Sensor-based globally asymptotically stable filters for attitude estimation: analysis, design, and performance evaluation. *IEEE Transactions on Automatic Control*, *57*(8), 2095–2100.

Batista, P., Silvestre, C., & Oliveira, P. (2019a). Globally exponentially stable attitude observer with earth velocity estimation. *Asian Journal of Control*.

Batista, P., Silvestre, C., & Oliveira, P. (2019b). Attitude observer on the special orthogonal group with Earth velocity estimation. *Systems & Control Letters*, *126*, 33–39.

Bijker, J., & Steyn, W. (2008). Kalman filter configurations for a low-cost loosely integrated inertial navigation system on an airship. *Control Engineering Practice*, *16*(12), 1509–1518.

Bitmead, R. R., & Gevers, M. (1991). Riccati difference and differential equations: convergence, monotonicity and stability. In *The Riccati Equation* (pp. 263–291). Springer Berlin Heidelberg.

Chang, L., Hu, B., & Li, K. (2016). Iterated multiplicative extended kalman filter for attitude estimation using vector observations. *IEEE Transactions on Aerospace and Electronic Systems*, *52*(4), 2053–2060.

Chang, L., Qin, F., & Li, A. (2015). A novel backtracking scheme for attitude determination-based initial alignment. *IEEE Transactions on Automation Science and Engineering*, *12*(1), 384–390.

Choukroun, D., Bar-Itzhack, I. Y., & Oshman, Y. (2006). Novel quaternion Kalman filter. *IEEE Transactions on Aerospace and Electronic Systems*, *42*(1), 174–190.

Grewal, M. S., & Andrews, A. P. (2010). Applications of kalman filtering in aerospace 1960 to the present [historical perspectives]. *IEEE Control Systems*, *30*(3), 69–78.

Grip, H. F., Fossen, T. I., Johansen, T. A., & Saberi, A. (2012). Attitude estimation using biased gyro and vector measurements with time-varying reference vectors. *IEEE Transactions on Automatic Control*, *57*(5), 1332–1338.

Khalil, H. K. (2002). *Nonlinear systems* (3rd ed.). New Jersey: Prentice Hall.

Khosravian, A., & Namvar, M. (2012). Rigid body attitude control using a single vector measurement and gyro. *IEEE Transactions on Automatic Control*, *57*(5), 1273–1279.

Kučera, V. (1973). A review of the matrix riccati equation. *Kybernetika*, *9*(1), 42–61.

Lefferts, E. J., Markley, F. L., & Shuster, M. D. (1982). Kalman filtering for spacecraft attitude estimation. *Journal of Guidance, Control and Dynamics*, *5*(5), 417–429.

de Marina, H. G., Pereda, F. J., Giron-Sierra, J. M., & Espinosa, F. (2012). UAV attitude estimation using unscented kalman filter and TRIAD. *IEEE Transactions on Industrial Electronics*, *59*(11), 4465–4474.

Markley, F. L. (1998). Attitude determination using two vector measurements. *NASA Technical Documents*.

Oshman, Y., & Markley, F. L. (1999). Spacecraft attitude/rate estimation using vector-aided GPS observations. *IEEE Transactions on Aerospace and Electronic Systems*, *35*(3), 1019–1032.

Reis, J., Batista, P., Oliveira, P., & Silvestre, C. (2018). Nonlinear attitude observer on SO(3) based on single body-vector measurements. In *2018 IEEE conference on control technology and applications*. IEEE.

Reis, J., Batista, P., Oliveira, P., & Silvestre, C. (2019). Nonlinear observer on SO(3) for attitude estimation on rotating earth using single vector measurements. *IEEE Control Systems Letters*, *3*(2), 392–397.

Rugh, W. J. (1996). *Linear system theory* (second ed.). NJ: Prentice Hall Upper Saddle River.

Sabatini, A. M. (2011). Kalman-filter-based orientation determination using inertial/magnetic sensors: observability analysis and performance evaluation. *Sensors*, *11*(10), 9182–9206.

Stojanovic, V., & Nedic, N. (2015). Robust Kalman filtering for nonlinear multivariable stochastic systems in the presence of non-Gaussian noise. *International Journal of Robust and Nonlinear Control*, *26*(3), 445–460.

Stovner, B. N., Johansen, T. A., Fossen, T. I., & Schjølberg, I. (2018). Attitude estimation by multiplicative exogenous kalman filter. *Automatica*, *95*, 347–355.

Wahba, G. (1965). A least squares estimate of satellite attitude. *SIAM Review*, *7*(3), 409.

Wu, J., Zhou, Z., Gao, B., Li, R., Cheng, Y., & Fourati, H. (2018). Fast linear quaternion attitude estimator using vector observations. *IEEE Transactions on Automation Science and Engineering*, *15*(1), 307–319.